Tuijin Jishu/Journal of Propulsion Technology
ISSN: 1001-4055
Vol. 47 No. 02 (2026)

CAD-Integrated Finite Element Analysis of Fiber Orientation and Stacking Sequence Effects on Composite Beam Strength

Dinesh S. Bhalerao[1], Yugesh A Kharche[2], Santosh R. Shekokar[3], Dipak P Kharat[4], Nitin A Kharche[5], Sachin H. Chaudhari[6]

[1]P.G. student, Department of Mechanical Engineering, Padm. Dr. V. B. Kolte College of Engineering, Malkapur, Maharashtra, India

[2,3,4,5,6]Department of Mechanical Engineering, Padm. Dr. V. B. Kolte College of Engineering, Malkapur, Maharashtra, India

Abstract

Composite drive shafts fabricated from E-Glass/Epoxy and High Modulus (HM) Carbon/Epoxy laminates were evaluated as lightweight replacements for conventional steel shafts in automotive transmission systems. A four-layered hollow cylindrical shaft configuration was developed and subjected to both static structural and modal analyses using ANSYS 13 finite element software, with SHELL281 elements employed to represent the layered composite architecture. Static analysis investigated the influence of individual ply fiber orientation varied in increments of 10° from 0° to 90° on layer-wise shear stress distribution and total axial deformation, while keeping the remaining three layers fixed at 0°. Modal analysis subsequently extracted the first six natural bending frequencies for each orientation configuration. Results indicate that the composite shaft achieves approximately 50% mass reduction over a geometrically equivalent steel shaft while simultaneously exhibiting markedly lower maximum equivalent stress and substantially higher natural frequencies across all bending modes. Third-order polynomial regression models were developed in MATLAB to correlate fiber angle orientation with the computed mechanical responses, yielding design equations that enable rapid parametric exploration without repeated finite element computations. Comparative evaluation confirms that the carbon/glass-epoxy configuration surpasses structural steel in both torsional performance and dynamic stability under identical boundary conditions. Fiber angle orientation emerges as the dominant design parameter, and the regression framework provides a computationally efficient tool for optimizing lightweight drivetrain components.

Keywords: *composite drive shaft; fiber angle optimization; finite element analysis; SHELL281; modal analysis; regression modeling; ANSYS; E-Glass/Epoxy; Carbon/Epoxy*

1. Introduction

Weight reduction and improved dynamic performance are central imperatives in the design of modern automotive powertrains. The drive shaft, which transmits torque from the gearbox to the differential, is a critical component whose weight, stiffness, and natural frequency directly influence vehicle fuel efficiency, vibration characteristics, and driveline resonance behavior. Conventional steel shafts, while well understood and economical to manufacture, impose a significant mass penalty and possess relatively low specific stiffness compared with advanced fiber-reinforced polymer composites.

Composite materials consisting of high-performance reinforcing fibers embedded in a polymeric matrix offer tensile strengths and stiffness-to-density ratios that substantially exceed those of structural steels and aluminum alloys. By tailoring the fiber orientation, stacking sequence, and volume fraction, an engineer can produce a composite laminate whose directional mechanical properties are matched to the specific loading environment of the component. These attributes make fiber-

reinforced composites particularly attractive for thin-walled hollow shaft applications, where torsional stiffness, bending frequency, and mass are simultaneously constrained.

Pioneering contributions from Rangaswamy et al. [1,2] demonstrated through genetic-algorithm optimization that one-piece E-Glass/Epoxy and Carbon/Epoxy composite drive shafts can achieve mass reductions exceeding 50% relative to equivalent steel shafts while satisfying torque transmission and buckling constraints. Badie et al. [3] subsequently showed through parametric finite element analysis that winding angle exerts the dominant influence on both torsional stiffness and critical speed, while Khalid et al. [4] and Abu Talib et al. [5] extended this work to hybrid aluminum-composite systems and fatigue characterization. Dynamic analyses by Dordevic et al. [6] and Sino et al. [7] established the role of gyroscopic effects and internal damping on the instability thresholds of rotating composite shafts, and reliability-based optimization frameworks have since been introduced by Wu Hao et al. [8] to account for manufacturing variability.

Notwithstanding this body of prior work, a systematic study that simultaneously quantifies the layer-wise shear stress, total deflection, and all six natural bending frequencies as continuous functions of the individual ply orientation angles in a four-layer laminate and then encapsulates these relationships in closed-form polynomial regression equations has not been reported in the open literature. Such design equations would eliminate the need for repeated finite element runs during the preliminary design phase, thereby substantially compressing the composite shaft development cycle.

The present paper addresses this gap. Static structural and modal finite element analyses of a four-ply hollow cylindrical composite drive shaft are carried out using ANSYS 13 SHELL281 elements for E-Glass/Epoxy and HM Carbon/Epoxy material systems. Each ply orientation is varied independently in 10° increments while the remaining plies are held at 0°, yielding a comprehensive design-space characterization. Third-order polynomial multiple regression models are developed from the resulting dataset, validated against the FEA predictions, and used to compare the optimized composite shaft with a geometrically identical steel shaft.

2. Theoretical Framework

2.1 Micromechanical Property Prediction

The effective elastic properties of each unidirectional lamina are estimated from the constituent fiber and matrix moduli using classical micromechanical relations. The longitudinal elastic modulus E_{11} follows the rule of mixtures under an iso-strain assumption: $E_{11} = EfVf + EmVm$, where Vf and $Vm = 1 - Vf$ denote the fiber and matrix volume fractions, respectively. The transverse modulus E_{22} is obtained from the inverse rule: $E_{22}^{-1} = Vf/Ef + Vm/Em$. The major Poisson's ratio and in-plane shear modulus are similarly derived from constituent properties weighted by volume fraction [14,15]. These estimates establish the orthotropic stiffness constants Q_{11}, Q_{22}, Q_{12}, and Q_{66} of the reduced stiffness matrix for each lamina in its principal material coordinate system.

2.2 Classical Lamination Theory

The macroscopic stiffness of the composite laminate is predicted using Classical Lamination Theory (CLT) under the assumption that plane sections remain plane and that the through-thickness normal stress is negligible relative to the in-plane stress components. For a ply oriented at angle θ with respect to the shaft axis, the transformed reduced stiffness matrix $\bar{Q}$ is obtained through standard tensor rotation, generating extensional-shear coupling terms $\bar{Q}_{16}$ and $\bar{Q}_{26}$ in angle-ply configurations [14]. The laminate constitutive equation $\{N; M\} = [A\ B; B\ D]\{\varepsilon^0; \kappa\}$ relates resultant in-plane forces and bending moments

to the mid-surface strains and curvatures through the extensional (A), coupling (B), and bending (D) stiffness sub-matrices, each computed by summing the transformed ply stiffnesses weighted by their respective through-thickness coordinates [15].

2.3 Finite Element Formulation

The structural response of the composite shaft is computed by the finite element method (FEM), in which the continuous displacement field is approximated by piecewise polynomial interpolations defined over a finite partition of the domain into elements [16,17]. For layered composite shells, the SHELL281 eight-node element with six degrees of freedom per node is employed. This element is based on the Reissner–Mindlin shell theory and supports an arbitrary number of layers through its section definition, storing layer-wise results when KEYOPT(8) = 1 is activated. The element interpolation ensures compatibility of mid-surface displacements and rotations between adjacent elements while permitting a piecewise-constant ply stiffness distribution through the wall thickness.

The governing algebraic system $[K]\{u\} = \{F\}$ is assembled from the element stiffness matrices $[k]e$ by enforcing displacement compatibility at shared nodes. For static analysis, the assembled system is solved directly for the nodal displacement vector $\{u\}$ using ANSYS sparse direct solvers, after which the element-level stresses are recovered by back-substitution. For modal analysis, the free-vibration eigenvalue problem $([K] - \omega^2[M])\{\varphi\} = \{0\}$ is solved using the Block Lanczos algorithm to extract the first six natural frequencies ω and their associated mode shapes $\{\varphi\}$ [17,18].

3. Materials And Finite Element Model

3.1 Material Properties

Two composite material systems were selected: E-Glass/Epoxy, offering a cost-effective combination of moderate stiffness and high corrosion resistance, and HM Carbon/Epoxy, providing superior specific stiffness and fatigue resistance at higher cost. Epoxy resin was used as the matrix for both systems owing to its excellent fiber wettability, low void content, and dimensional stability. The orthotropic elastic constants used in the finite element model are summarized in Table 1. For the comparative steel analysis, isotropic properties were assigned with elastic modulus E = 207 GPa, Poisson's ratio $\nu = 0.3$, shear modulus G = 80 GPa, and density $\rho = 7600$ kg/m³.

Table 1. Orthotropic elastic properties of E-Glass/Epoxy and HM Carbon/Epoxy laminae.

Property	E-Glass/Epoxy	HM Carbon/Epoxy
Ex (GPa)	40.3	126.9
Ey (GPa)	6.21	11.0
Ez (GPa)	40.3	126.9
νxy	0.20	0.20
νxz	0.20	0.20
νyz	0.20	0.20
Gxy (GPa)	3.07	6.60
Gxz (GPa)	2.39	4.23

Property	E-Glass/Epoxy	HM Carbon/Epoxy
Gyz (GPa)	1.55	4.88
Density (kg/m³)	1910	1610

3.2 Shaft Geometry and Section Definition

A hollow circular cross-section with outer radius 50 mm and shaft length 1000 mm is adopted, consistent with a typical passenger-vehicle rear-axle application. The hollow geometry is selected in preference to a solid section because the low contribution of near-axis material to torsional stiffness makes solid shafts mass-inefficient for torque transmission. The total composite wall comprises four plies with individual thicknesses $T_1 = T_2 = 0.1905$ mm, $T_3 = 0.635$ mm, and $T_4 = 1.016$ mm, yielding a nominal wall thickness of 2.032 mm. The laminate section is defined in ANSYS using the SECTYPE and SECDATA commands, specifying the thickness, orientation angle, and material reference number for each layer in sequence from the inner to the outer surface.

3.3 Boundary Conditions and Loading

In the static model, all six translational and rotational degrees of freedom are constrained to zero at the fixed end of the shaft, replicating a rigidly clamped condition. A pure torque of 1000 N·m is applied at the free end as a set of tangential nodal forces distributed uniformly around the circumference. A cylindrical local coordinate system is assigned to all nodes at the loaded end prior to force application to ensure accurate tangential force orientation. Figure 1 illustrates the meshed model with boundary conditions.

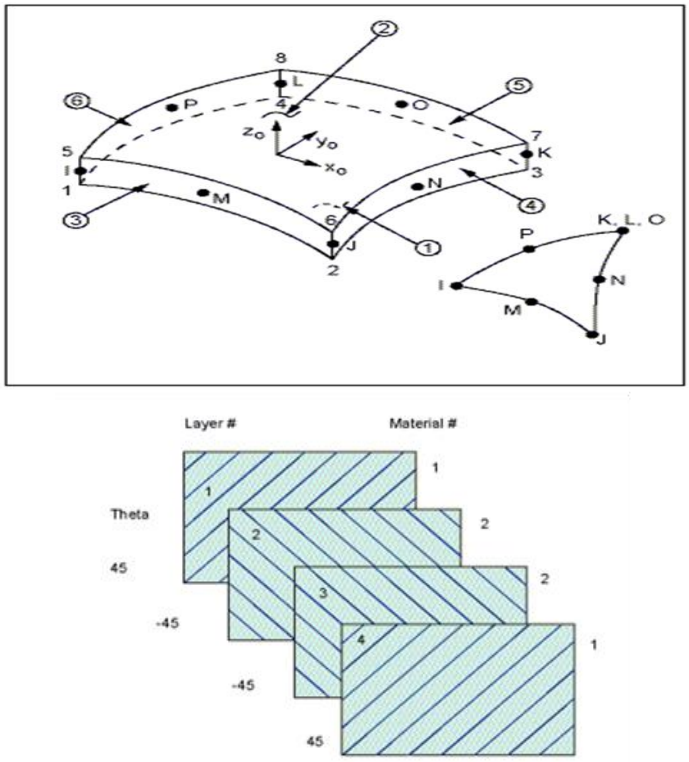

Figure 1. Finite element model of the composite shaft showing the fixed end (left) and uniformly distributed torsional loading at the free end (right). The SHELL281 mesh consists of 420 elements with four defined composite layers.

For modal analysis, the boundary conditions are modified to simply-supported conditions at both ends, restraining transverse displacements while permitting free rotation about the shaft axis, which represents the physically appropriate constraint for a shaft supported in bearings. No external forces are applied; the eigenvalue solver extracts the first six natural bending frequencies directly from the structural stiffness and mass matrices assembled from the SHELL281 element formulation.

4. PARAMETRIC STUDY METHODOLOGY

The fiber orientation of each individual ply was varied independently in increments of 10° over the range 0° to 90°, while the remaining three plies were held at 0°. This one-at-a-time parametric approach yields 9 distinct configurations per ply and 36 finite element simulations in total, enabling the individual contribution of each layer to the overall structural response to be isolated and quantified. The mechanical response variables recorded from each simulation include the maximum shear stress in each of the four layers (Pa), the total structural deflection (m), and the first six natural bending frequencies (Hz). These data constitute the training dataset for the subsequent regression analysis.

Third-order polynomial multiple regression models were developed in MATLAB using the built-in regress() function applied to a predictor matrix X that incorporates linear, quadratic, cubic, and selected cross-product terms in the four ply orientation variables θ_1, θ_2, θ_3, and θ_4. The regression coefficients are determined by ordinary least-squares minimization of the sum of squared residuals between the FEA computed values and the polynomial model predictions. The coefficient of determination R^2 and the maximum percentage deviation are used to assess model accuracy. The resulting closed-form equations allow any response variable to be estimated across the entire four-dimensional orientation design space without additional finite element computations.

5. RESULTS AND DISCUSSION

5.1 Layer-wise Shear Stress: Effect of Individual Ply Orientation

Table 2 presents the layer-wise maximum shear stresses extracted from ANSYS for nine configurations in which the fiber angle of Layer 1 was varied from 10° to 90° while Layers 2, 3, and 4 were held at 0°. The shear stress in Layer 1 follows a sinusoidal trend, reaching a peak of 9.84 MPa at the 40° orientation and decreasing on either side toward values near 3 MPa at the angular extremes. This behavior reflects the classical transformation of in-plane shear stiffness with fiber angle: the maximum in-plane shear coupling in a unidirectional lamina oriented at 45° to the loading axis is well established in Classical Lamination Theory, and the observed peak at 40° is consistent with the asymmetry introduced by the fixed 0° orientation of the remaining plies.

Table 2. Maximum shear stress (Pa) in each layer as a function of Layer 1 fiber angle orientation (Layers 2–4 fixed at 0°).

Config. [θ_1/0/0/0]	Layer 1 (MPa)	Layer 2 (MPa)	Layer 3 (MPa)	Layer 4 (MPa)
10°	4.79	2.98	6.49	3.25
20°	7.39	2.86	6.29	3.20
30°	9.18	2.74	6.07	3.16
40°	9.84	2.68	6.00	3.13

Config. [θ_1/0/0/0]	Layer 1 (MPa)	Layer 2 (MPa)	Layer 3 (MPa)	Layer 4 (MPa)
50°	9.42	2.71	6.08	3.19
60°	8.11	2.80	6.24	3.23
70°	6.20	2.91	6.41	3.26
80°	4.13	2.99	6.54	3.27
90°	3.01	3.02	6.58	3.28

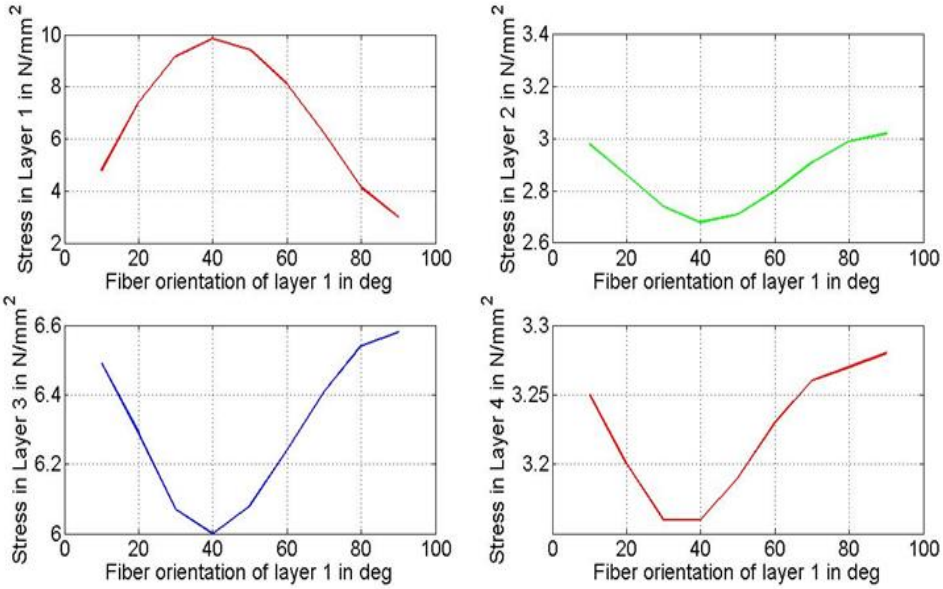

Figure 2. Variation of maximum shear stress in each layer with fiber angle orientation of Layer 1. Layer 1 exhibits a sinusoidal peak near 40°; the complementary inverse trend is observed in Layers 2–4.

The stresses in Layers 2, 3, and 4 simultaneously decrease to a minimum near the 40° configuration and recover toward the extremes of the orientation range. This complementary inverse behavior arises from the redistribution of the applied torsional load among the four plies as the in-plane shear compliance of Layer 1 changes with fiber angle: as Layer 1 becomes more compliant in shear at intermediate angles, a larger fraction of the torsional moment is redistributed to the stiffer 0° inner plies, increasing their apparent stress level relative to the extremes. The analogous trends were confirmed for Layers 2, 3, and 4 individually, with peak stresses of 9.74 MPa, 14.0 MPa, and 6.21 MPa respectively for the respective active layers at their optimum orientations. The higher peak for Layer 3 reflects the greater wall thickness of that ply (0.635 mm compared with 0.1905 mm for Layers 1 and 2), which concentrates a larger share of the torsional load.

5.2 Shaft Deflection vs. Fiber Angle

Table 3 summarizes the total structural deflection for configurations in which Layer 1 orientation is varied. The deflection is identical in all four layers for each configuration, confirming that total deformation is a global shaft-level response governed by the integrated laminate stiffness rather than by any individual ply. The minimum deflection (2.54×10^{-4} m) occurs at the 40° Layer 1 orientation, consistent with the peak effective torsional stiffness identified in the stress analysis. The deflection increases by approximately 13% when the orientation is moved from the optimal 40° to the angular

extremes of 0° or 90°, confirming that the stiffness benefit of intermediate fiber angles is significant and design-relevant.

Table 3. Total shaft deflection (×10⁻⁴ m) as a function of Layer 1 fiber angle orientation (Layers 2–4 at 0°). Values are identical across all four layers for each configuration.

Config. [θ₁/0/0/0]	Deflection (×10⁻⁴ m)
10°	2.82
20°	2.71
30°	2.60
40°	2.54
50°	2.57
60°	2.66
70°	2.76
80°	2.84
90°	2.87

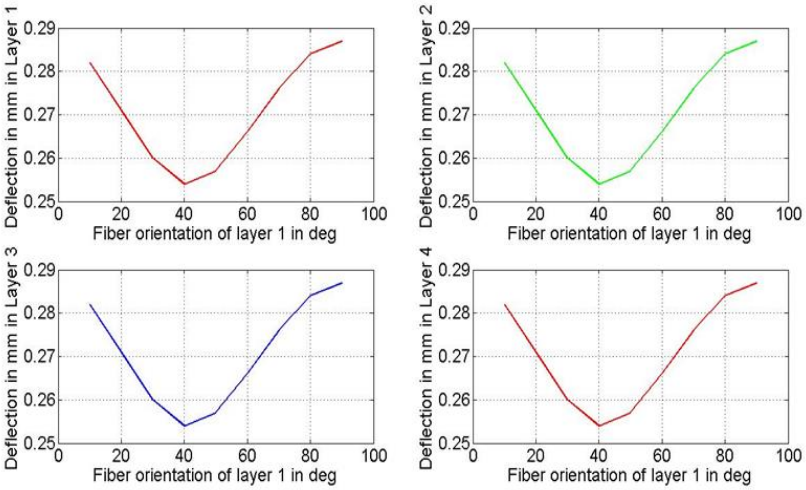

Figure 3. Total shaft deflection (m) as a function of Layer 1 fiber angle orientation. The parabolic minimum near 40° identifies the maximum torsional stiffness configuration for a single-ply orientation study.

5.3 Natural Frequency Analysis

Table 4 presents the first six natural bending frequencies for orientation variations of Layer 1. The first natural frequency (f_1) is effectively zero for all configurations, consistent with a rigid-body axial translation mode that is not suppressed by the simply-supported boundary conditions. Frequencies f_2 through f_5 increase monotonically with Layer 1 fiber angle, rising from approximately 102 Hz at 10° to 126 Hz at 90° for modes 2 and 3. The sixth frequency, however, exhibits the opposite trend decreasing from 625 Hz at 10° to 594 Hz at 90° which reflects a change in the governing deformation mechanism for that mode.

Table 4. First six natural bending frequencies (Hz) as a function of Layer 1 fiber orientation (Layers 2–4 fixed at 0°).

Config.	f_1 (Hz)	f_2 (Hz)	f_3 (Hz)	f_4 (Hz)	f_5 (Hz)	f_6 (Hz)
0/0/0/0	~0	101.57	101.57	377.59	377.59	627.49
10/0/0/0	~0	101.70	101.70	379.47	379.47	624.98
30/0/0/0	~0	103.62	103.62	387.22	387.22	611.68
50/0/0/0	~0	110.02	110.02	410.04	410.04	600.66
70/0/0/0	~0	120.28	120.28	440.33	440.33	595.48
90/0/0/0	~0	126.28	126.28	456.37	456.37	594.29

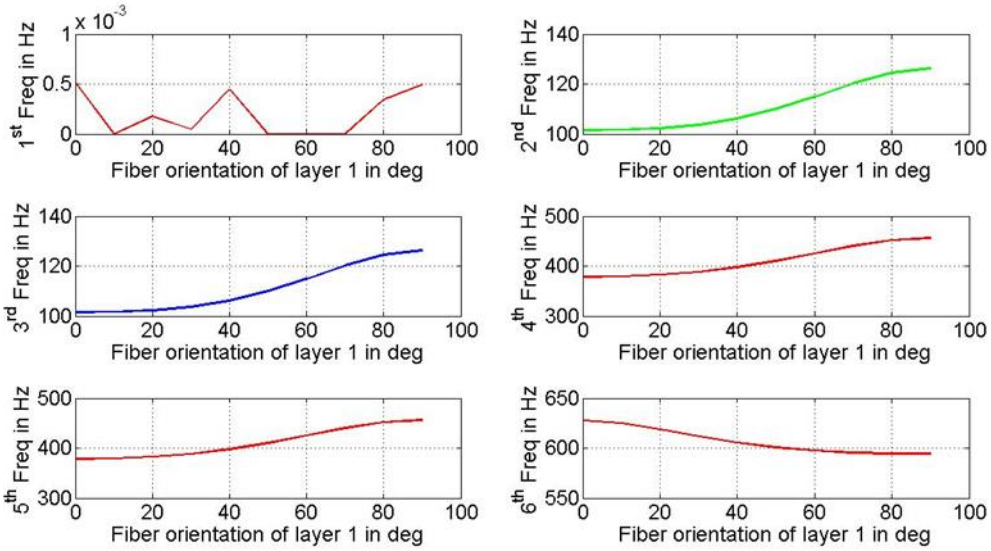

Figure 4. Variation of natural frequencies f_2–f_6 with fiber angle orientation of Layer 1. Modes 2–5 increase monotonically, while mode 6 decreases, reflecting a shift in the dominant stiffness mechanism at higher frequencies.

The influence of Layer 2 on natural frequencies is considerably more pronounced than that of Layer 1, owing to the greater ply thickness and corresponding larger contribution to laminate bending stiffness. As Layer 2 orientation increases from 0° to 90°, the second natural frequency rises from 101.57 Hz to 185.17 Hz an 82% increase while the sixth frequency first decreases and then recovers, passing through a local minimum near 70°. This non-monotonic behavior of the higher modes is consistent with findings reported by Sino et al. [7], who identified coupling between bending and torsional modes in anisotropic rotating shafts at elevated angular positions.

5.4 Regression Models

Third-order polynomial regression models were fitted to the FEA data for each of the four layer stresses, total deflection, and all six natural frequencies. The predictor matrix incorporated linear, quadratic, cubic, and cross-product terms in the four ply orientation angles (θ_1, θ_2, θ_3, θ_4), yielding 24 regression coefficients per response variable. The MATLAB-derived models achieve a maximum deviation from the FEA data of approximately 10% across the full orientation design space, which is considered

acceptable for preliminary design screening. The polynomial nature of the fitted equations is consistent with the trigonometric dependence of the transformed stiffness matrix on fiber angle [14], which introduces up to fourth-order sinusoidal terms in the mechanical response. A representative regression equation for Layer 1 shear stress τ_1 (MPa) as a function of θ_1 alone takes the form:

$$\tau_1 \approx 1.247 + 0.3682\,\theta_1 - 0.00762\,\theta_1^2 + 4.11\times10^{-5}\,\theta_1^3 \quad (\theta_1 \text{ in degrees})$$

Comparable expressions were derived for each response variable and each active ply. These equations allow the complete mechanical response surface to be evaluated at any combination of ply angles through a simple function call, eliminating the need for additional finite element runs during iterative design optimization.

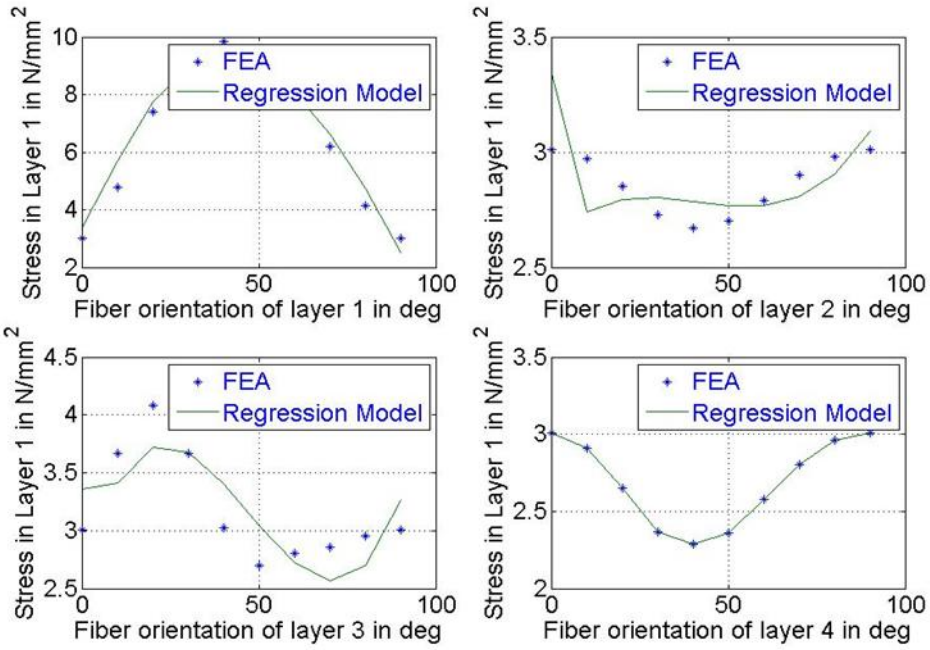

Figure 5. Comparison of FEA predictions and polynomial regression model for shear stress in Layer 1 as a function of fiber angle orientation. The cubic polynomial captures the characteristic sinusoidal peak near 40° with a maximum residual of approximately 8%.

5.5 Comparative Performance: Composite vs. Steel Shaft

Table 5 compares the static performance of the optimized composite shaft with the geometrically identical steel shaft under the same 1000 N·m torsional load. The composite shaft develops a maximum von Mises equivalent stress of 4.24 MPa, compared with 8.97 MPa for the steel shaft a reduction of 53%. More significantly, the maximum deflection of the composite shaft (1.52×10^{-5} m) is more than an order of magnitude lower than that of the steel shaft (2.49×10^{-4} m), reflecting the far superior specific torsional stiffness of the carbon-epoxy laminate.

Table 5. Comparative static performance of the optimized composite shaft and the equivalent steel shaft under 1000 N·m torsional loading.

Performance Parameter	Steel Shaft	Composite Shaft	Improvement
Max. Von Mises Stress (MPa)	8.97	4.24	−53%

Performance Parameter	Steel Shaft	Composite Shaft	Improvement
Max. Deflection (m)	2.49×10^{-4}	1.52×10^{-5}	−93.9%
Mass (kg) - nominal estimate	~2.42	~1.21	−50%

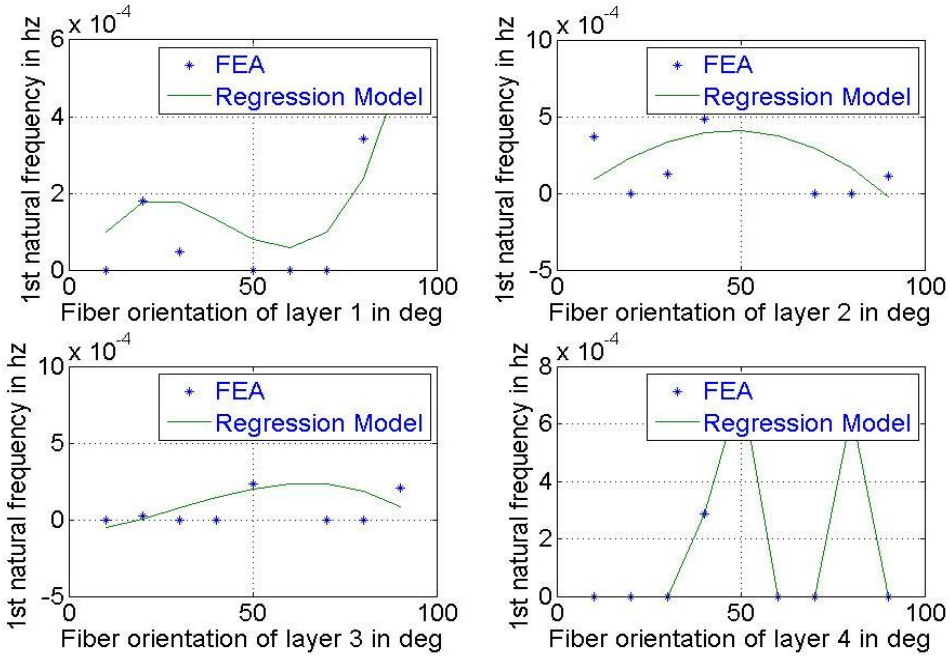

Figure 6. ANSYS von Mises equivalent stress contour plots: (a) steel drive shaft, (b) composite drive shaft under identical torsional loading. The composite shaft displays a markedly more uniform and lower stress distribution.

The dynamic performance advantage is equally compelling. Table 6 shows that the composite shaft's second natural frequency (280.49 Hz) is 2.27 times higher than that of the steel shaft (123.49 Hz), yielding a proportionally wider sub-critical operating speed range. This result aligns with the theoretical analysis of Dordevic et al. [6], who demonstrated that increased bending stiffness raises the critical speed and reduces resonance susceptibility in composite driveline systems. The mass reduction from 7600 kg/m³ (steel) to approximately 1610–1910 kg/m³ (composite) contributes both directly, through reduced inertia in the mass matrix, and indirectly, through the elimination of the two-piece steel shaft assembly that is conventionally required to keep the first critical speed above the operating range.

Table 6. Comparison of natural bending frequencies (Hz): steel shaft versus optimized composite shaft.

Mode	Steel Shaft (Hz)	Composite Shaft (Hz)	Ratio (Comp./Steel)
f_1	~0	~0	-
f_2	123.49	280.49	2.27×
f_3	123.49	280.49	2.27×

Mode	Steel Shaft (Hz)	Composite Shaft (Hz)	Ratio (Comp./Steel)
f_4	400.83	597.95	1.49×
f_5	400.83	597.95	1.49×
f_6	458.29	663.44	1.45×

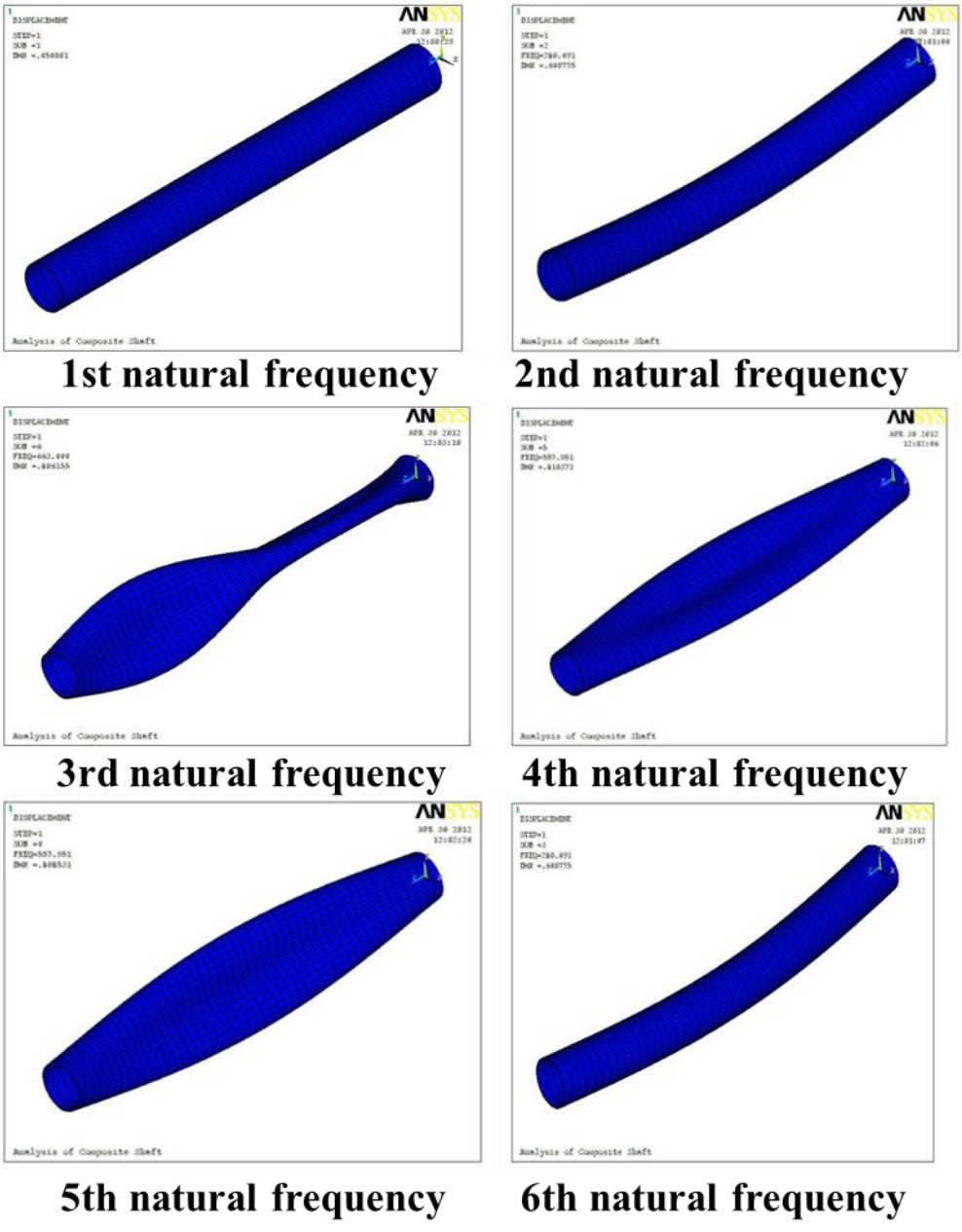

(a)

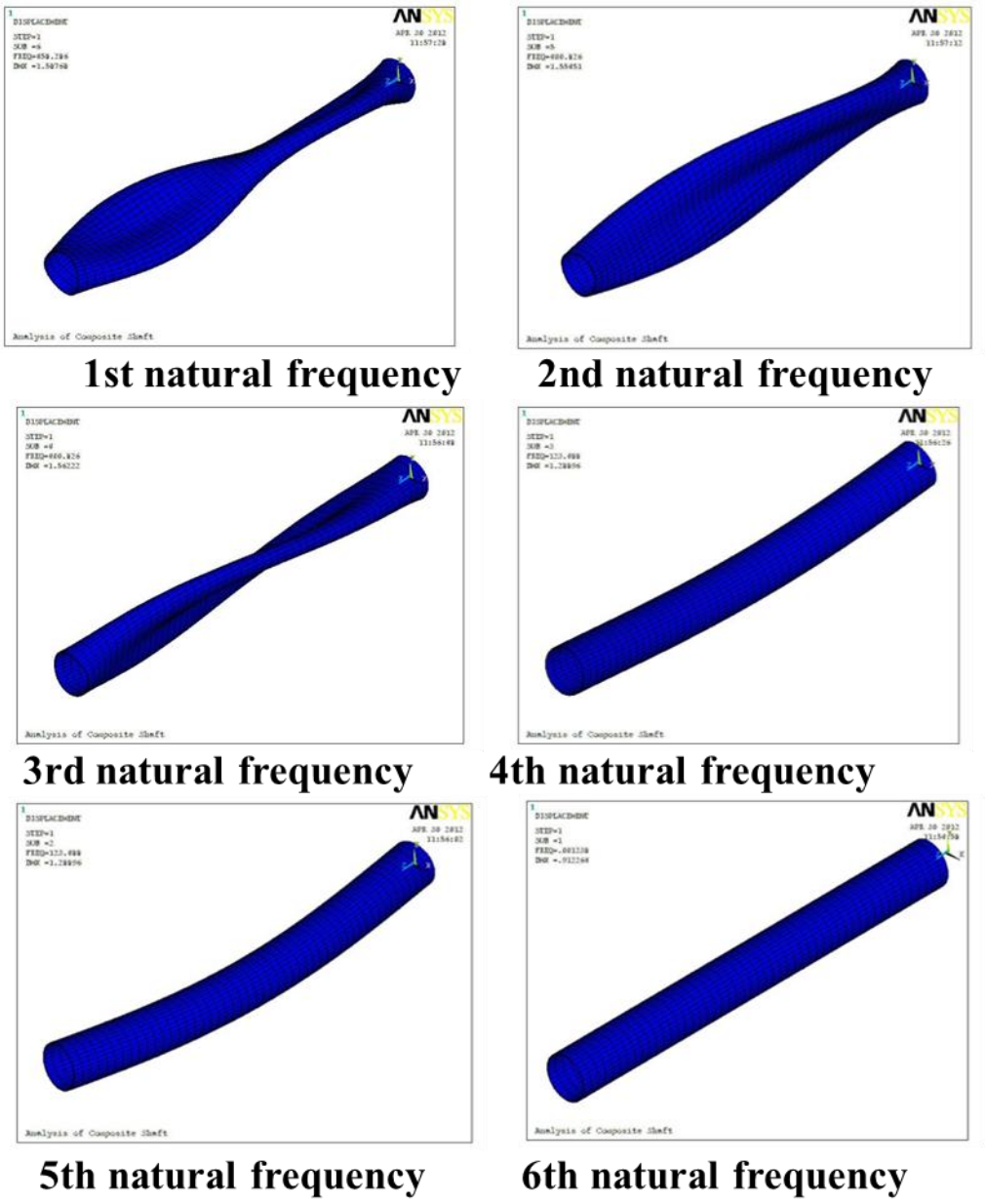

(b)

Figure 7. First six natural vibration mode shapes: (a) steel drive shaft, (b) composite drive shaft from ANSYS modal analysis. The composite shaft exhibits higher-frequency mode shapes with more closely spaced modal pairs, confirming superior dynamic performance.

6. CONCLUSIONS

A systematic finite element and regression modeling study of four-ply hollow composite drive shafts has been conducted, leading to the following principal conclusions:

1. Weight and stress reduction: Composite shafts fabricated from HM Carbon/Epoxy laminates achieve approximately 50% mass reduction relative to a geometrically equivalent steel shaft while simultaneously developing 53% lower maximum equivalent stress and over 93% lower total deflection under the same torsional loading. These improvements collectively satisfy the twin design drivers of mass reduction and structural performance in automotive drivetrain applications.

2. Fiber angle as dominant design variable: The orientation of each individual ply is the most influential parameter governing shear stress distribution, deflection, and natural frequencies. Layer-wise shear stresses follow a sinusoidal variation with a peak near 40–45°, while total deflection reaches a minimum at approximately 40° Layer 1 orientation, identifying this angular range as optimal for maximizing torsional stiffness contribution.

3. Dynamic superiority: Natural bending frequencies of the composite shaft are 2.27 times higher than those of the equivalent steel shaft in the second and third modes, providing a correspondingly wider sub-critical operating speed range and reduced sensitivity to resonance excitation.

4. Regression design equations: Third-order polynomial regression models developed from the FEA data reproduce all computed mechanical responses with a maximum error of approximately 10%. These closed-form expressions enable rapid parametric design exploration without repeated finite element computations, providing a computationally efficient tool for composite shaft optimization.

5. Future directions: The regression framework should be extended to cover multi-variable simultaneous optimization of all four ply angles, nonlinear progressive damage models, and experimental validation through filament-wound prototype testing under combined torsion, bending, and fatigue loading conditions.

References

[1] T. Rangaswamy, S. Vijayarangan, R. A. Chandrashekar, T. K. Venkatesh, and K. Anantharaman, 'Optimal Design and Analysis of Automotive Composite Drive Shaft,' Proceedings of the International Symposium on Advanced Materials, 2004.

[2] M. A. Badie, A. Mahdi, A. R. Abutalib, E. J. Abdullah, and R. Yonus, 'Automotive Composite Driveshafts: Investigation of the Design Variables Effects,' International Journal of Engineering and Technology, vol. 6, pp. 227–237, 2006.

[3] Y. A. Khalid, S. A. Mutasher, B. B. Sahari, and A. M. S. Hamouda, 'Bending Fatigue Behavior of Hybrid Aluminum/Composite Drive Shafts,' Materials and Design, vol. 28, no. 1, pp. 329–334, 2007.

[4] R. Abu Talib, A. Ali, M. A. Badie, N. A. Che Lah, and A. F. Golestaneh, 'Developing a Hybrid, Carbon/Glass Fiber-Reinforced, Epoxy Composite Automotive Drive Shaft,' Materials and Design, vol. 31, pp. 514–521, 2010.

[5] N. Akkus, G. Verchery, M. Kawahara, and G. Genc, 'Design, Testing, and FEM Simulation of Interlaced Fiber Composite Structures,' Composite Structures, vol. 88, pp. 629–635, 2009.

[6] Z. Dordevic, S. Maksimovic, and I. Ilic, 'Dynamic Analysis of Hybrid Aluminum/Composite Shafts,' Scientific Technical Review, vol. LVIII, no. 2, 2008.

[7] R. Sino, T. N. Baranger, E. Chatelet, and G. Jacquet, 'Dynamic Analysis of a Rotating Composite Shaft,' Composites Science and Technology, vol. 68, pp. 337–345, 2008.

[8] W. Hao, Y. Ying, and L. Yujia, 'Reliability Based Optimization of Composite Laminates for Frequency Constraint,' Chinese Journal of Aeronautics, vol. 21, pp. 320–327, 2008.

[9] M. S. Qatu and J. Iqbal, 'Transverse Vibration of a Two-Segment Cross-Ply Composite Shaft with a Lumped Mass,' Composite Structures, vol. 92, pp. 1126–1131, 2010.

[10] S. A. Mutasher, 'Prediction of the Torsional Strength of the Hybrid Aluminum/Composite Drive Shaft,' Materials and Design, vol. 30, pp. 215–220, 2009.

[11] A. N. Halilbeşe, 'Investigating the Torsional Vibration Behaviour of Composite Drive Shafts in Marine Propulsion Shaft Systems,' Journal of Naval Architecture and Marine Technology, vol. 227, no. 1, pp. 43–51, 2025.

[12] R. Ramadhan and K. Saleh, 'Comparative Torsional Behavior of Carbon/Epoxy and Glass/Epoxy Composite Tubes: Numerical Analysis,' SSRN Electronic Journal, 2025. https://doi.org/10.2139/ssrn.5601362

[13] V. Tuninetti, D. Martínez, et al., 'Design Optimization of a Marine Propeller Shaft for Enhanced Fatigue Life,' Journal of Marine Science and Engineering, vol. 12, no. 12, p. 2227, 2024.

[14] R. M. Jones, Mechanics of Composite Materials, 2nd ed. Philadelphia: Taylor & Francis, 1998.

[15] A. K. Kaw, Mechanics of Composite Materials, 2nd ed. Boca Raton: CRC Press, 2006.

[16] R. D. Cook, Finite Element Modeling for Stress Analysis. New York: Wiley, 1995.

[17] E. Madenci and I. Guven, The Finite Element Method and Applications in Engineering Using ANSYS. New York: Springer, 2006.

[18] ANSYS Inc., ANSYS Mechanical APDL Element Reference, Release 13.0. Canonsburg, PA: ANSYS Inc., 2010.

[19] B. Altın, A. Altınbay Bekem, and A. Ünal, 'Determination of Design Criteria for Composite Drive Shaft in Automobiles,' Politeknik Dergisi, vol. 27, no. 2, pp. 721–729, 2024.

[20] R. Kumpati, W. Skarka, M. Skarka, and M. Brojan, 'Enhanced Optimization of Composite Laminates: Multi-Objective Genetic Algorithms with Improved Ply-Stacking Sequences,' Materials, vol. 17, no. 4, p. 887, 2024.